ELSEVIER

Journal of Molecular Catalysis A: Chemical 152 (2000) 201–212

JOURNAL OF MOLECULAR CATALYSIS A: CHEMICAL

www.elsevier.com/locate/molcata

# Reactions of ethanol over metal oxides

H. Idriss [a,*], E.G. Seebauer [b]

[a] *Materials Chemistry, Department of Chemistry, The University of Auckland, Private Bag 92019, Auckland, New Zealand*
[b] *Department of Chemical Engineering, University of Illinois, Urbana, IL 61801, USA*

Received 23 February 1999; accepted 2 July 1999

**Abstract**

The reaction of ethanol over a series of oxides ($Fe_2O_3$, $Fe_2O_3$/CaO, $Fe_3O_4$, $TiO_2$, CaO, and $SiO_2$) has been investigated. The main reaction product in all cases is acetaldehyde, with secondary products acetone and ethyl acetate. At 473 K, the rate constant k decreases according to the series $Fe_2O_3 > Fe_3O_4 > CaO > TiO_2 \gg SiO_2$. Titration of basic sites by $CO_2$ adsorption at room temperature shows that the reaction rate can be successfully normalised by basic site density for oxides that adsorb $CO_2$ except for CaO. Acetone production, presumably via acetate ketonization, is highest over $TiO_2$ while ethyl acetate formation, by Tishchenko reaction, is highest over $Fe_2O_3$. 

*Keywords:* Reactions; Ethanol; Metal oxides

## 1. Introduction

The reactions of ethanol on catalytic materials have been investigated for more than three decades [1–3]. These studies have been motivated by both the importance of ethanol in several industrial processes and its utility for fundamental studies of oxide and metal surfaces. From the perspective of applications, ethanol can be catalytically produced from ethylene on acidic catalysts [4] and from syngas using Rh-promoted $V_2O_5$ [5], $TiO_2$ [6] and $CeO_2$ [7]; alkali-promoted Pd on $CeO_2$ [8]; and Cu–Co [9]. As an end product, ethanol finds use as a fuel additive [10,11]. As a chemical intermediate, ethanol serves as a feedstock for acetaldehyde production via oxidative dehydrogenation using catalysts like Ag [12], CuO alone [13] or doped with other transition metals [14–16], $MnO_x$ [17], $MoO_3$ [18–22] and $CeO_2$ [23]. Condensation of two acetaldehyde molecules into crotonaldehyde [24] then leads to further production of various specialty chemicals. Ethanol also serves as a feedstock for the Lebedev process for making butadiene on $MgO/SiO_2$ catalysts [25]. More recently, ethanol has also been seriously considered as a viable pure source for green $H_2$-production, particularly because ethanol can be manufactured from biomass [26].

From the perspective of fundamental reactivity, ethanol provides a useful test material for assessing the tendency of a catalyst to drive dehydration (to ethylene) versus dehydrogenation (to acetaldehyde) [27,28]. In particular, ethanol has found considerable utility in ultra-

* Corresponding author.

1381-1169/00/$ - see front matter 
PII: S1381-1169(99)00297-6

high vacuum studies of metals having well-defined crystallographic orientations [29–33]. On oxide powders, work has remained limited mainly to catalysts showing potential for real applications, i.e., CuO-based catalysts [13–16], $MoO_3$ [18–22] and $TiO_2$ [34–36]. Reaction pathways have been interpreted in terms of bond strengths within the ethanol molecule [33,37] and within the solid surface [38], geometry and coordination environment of the surface metal cations [18–22,39,40], and acidity or basicity of adsorption sites [41–43]. However, the small data set raises questions about how reliable and general some of these interpretations are.

This present article attempts to firm up those conclusions by examining a wider range of oxides, including $SiO_2$, $TiO_2$, $Fe_2O_3$, $Fe_3O_4$, CaO and $Fe_2O_3$–CaO. We find that in all cases ethanol tends to dehydrogenate to acetaldehyde, which for some oxides in turn reacts further to acetone and/or ethyl acetate. Small amounts of methanol from ethanol reaction are also observed. Normalisation of ethanol reaction rate by the total number of sites adsorbing $CO_2$ (referred to as basic sites) succeeds within certain limits. In a related article [44], we analyse the rate data obtained in this work in terms of various thermodynamic and spectroscopic properties of the oxides.

## 2. Experiment

All experiments were conducted at the University of Illinois. Reactions were run in a fixed-bed microreactor having a volume of 8 ml. This reactor connected to an on-line gas chromatograph (Perkin Elmer 2000) equipped with flame ionisation and thermal conductivity detectors, and to a differentially pumped high-vacuum chamber equipped with a Dycor mass spectrometer (range up to 200 amu).

In a typical experiment, the reactor was charged with 250 mg of catalyst. All catalysts were heated before experimentation to a temperature of 523 K for 2 h. Ultrapure ethanol was placed into a saturator and kept at 273 K, yielding a vapor pressure of $1.5 \times 10^3$ Pa. Dry air flowed through the saturator to yield an effluent composition ratio $N_2$:$O_2$:ethanol of 78.8:19.6:1.5. For experiments performed with different $O_2$ concentrations, He was added to dilute this reactant to the desired level. Products were separated using a 1/8 in.-diameter, 6 ft long Chromosorb 102 column ramped at 3°C/min from 70 to 200°C. All product concentrations were calibrated using external standards.

$Fe_2O_3$, $Fe_3O_4$ and $TiO_2$ (anatase) were obtained from Fisher, and $SiO_2$ from Davison. CaO was produced from $Ca(OH)_2$ (Fisher) by annealing for 1 h at 580°C followed by 3 h at 750°C. These solids were characterised by standard methods to determine bulk structure, surface area, and surface composition. X-ray diffraction of the Fe oxides and $TiO_2$ was performed using a Rigaku Geigerflux diffractometer with a fine-focus Cu tube (45 keV, 20 mA). $Fe_2O_3$ exhibited the (104) and (110) diffraction lines characteristic of hematite. Similarly, $Fe_3O_4$

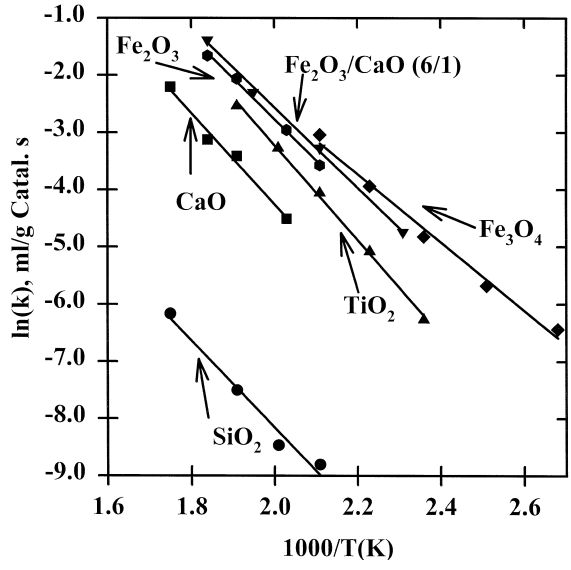


Fig. 1. Arrhenius plots of rate constant $k$ (ml/g s) for ethanol conversion normalised by mass.

Table 1
Arrhenius parameters for ethanol oxidation over oxides

| Oxide | $E_a$ (kJ/mol) | $A$ (ml/g s) | References |
|---|---|---|---|
| $Fe_3O_4$ | 48.6 | $1.2\times10^4$ | This work |
| $Fe_2O_3$ | 59.6 | $9.6\times10^4$ | This work |
| $TiO_2$ | 76.2 | $6.5\times10^5$ | This work |
| $TiO_2$[a] | 85 | – | [73] |
| CaO | 61 | $1.2\times10^5$ | This work |
| $SiO_2$ | 104.8 | $1\times10^3$ | This work |
| $CaO/Fe_2O_3$ | 59.3 | $1\times10^5$ | This work |
| $CeO_2$ | 75.4 | $3.8\times10^9$ | [23] |
| CuO | 50.6 | $3.1\times10^5$ | [13] |
| $MoO_3$ | 129 | – | [18] |

[a] Isopropanol.

showed peaks at $2\theta = 35.5°$ (311) and $2\theta = 62.8°$ (440) characteristic of magnetite. Finally, $TiO_2$ exhibited a (101) peak at $2\theta = 25.3°$ characteristic of anatase, with no evidence of a rutile phase. Surface areas were determined by 3-point BET experiments using an Autosorb-1. The surface areas in $m^2/g$ were 10.6 for $Fe_2O_3$, 7.3 for $Fe_3O_4$, 10.0 for $TiO_2$, 300 for $SiO_2$, and 10.0 for CaO. We have published elsewhere a characterisation of surface composition by X-ray photoelectron spectroscopy (XPS) [45]. In summary, the surfaces of both $Fe_2O_3$ and $Fe_3O_4$ seem composed of only $Fe^{+3}$ cations at 712.0 $\pm$ 0.1 eV ($Fe^{2+}$ of FeO are at 709.6 eV [45]). The XPS O(1s) showed that surface hydroxyls at 532.5 $\pm$ eV are considerably more pronounced on $Fe_3O_4$ than on $Fe_2O_3$. $TiO_2$ showed only $Ti^{+4}$ cations at 459.3 eV with a higher corrected O(1s) to Ti(2p) atomic ratio of 2.56 than stoichiometry. All spectra are corrected to residual C at 284.7 eV.

Table 2
$CO_2$ uptake of oxides

| Oxide | $CO_2$ uptake (molecules/$m^2$) |
|---|---|
| $TiO_2$ | $1.4\times10^{17}$ |
| $Fe_2O_3$ | $5.0\times10^{17}$ |
| $Fe_3O_4$ | $6.5\times10^{17}$ |
| CaO | $30.2\times10^{17}$ |
| $Fe_2O_3/CaO$ | $6.6\times10^{17}$ |
| Si $O_2$ | 0 |

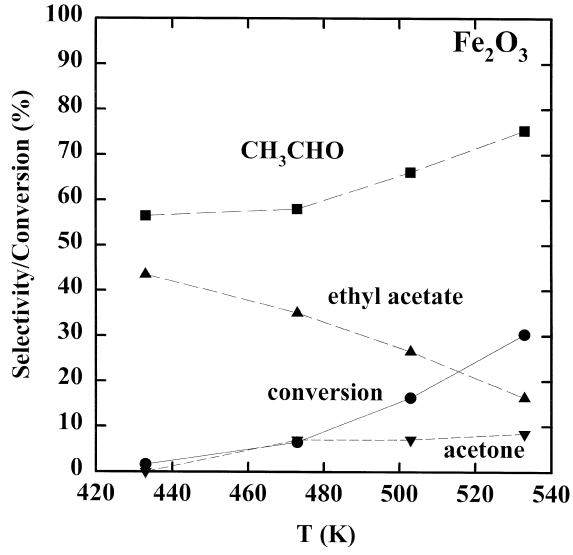


Fig. 2. Selectivity and conversion as a function of reaction temperature for ethanol reactions over $Fe_2O_3$.

The density of basic sites was also characterised via $CO_2$ titration. We employed a pulsing technique in which 0.5 ml of pure $CO_2$ at atmospheric pressure was introduced over 0.5 g of catalyst at room temperature. The outlet of the reactor was connected directly to a thermal conductivity detector to monitor the uptake.

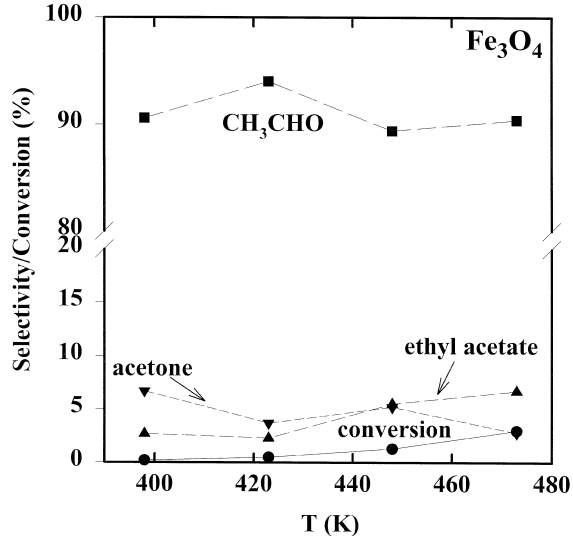


Fig. 3. Selectivity and conversion as a function of reaction temperature for ethanol reactions over $Fe_3O_4$.

## 3. Results

### 3.1. Rates

For all oxides the second order rate constant k was calculated from experimental data according to the following expression:

$$r = k[\text{Ethanol}]_{\text{out}}[\text{Oxide}] \quad (1)$$

First-order behavior with respect to ethanol was confirmed in the case of $Fe_2O_3$ by examining the variation of conversion $x$ with flowrate $F$ at constant oxygen concentration. First-order kinetics in a well-mixed reactor relate these quantities through:

$$\ln(1/(1-x)) = kW/F \quad (2)$$

where $x = ([\text{EtOH}]_{\text{in}} - [\text{EtOH}]_{\text{out}})/[\text{EtOH}]_{\text{in}}$, and $W$ denotes the weight of catalyst. Similar experiments with fixed ethanol concentration ($2 \times 10^{-6}$ mol/ml) and variable oxygen concentration (between 5 and 20%) showed a weak dependence of the reaction rate, with a computed order of 0.11 with respect to oxygen. The oxygen concentration was kept constant at 19.6% for all remaining experiments.

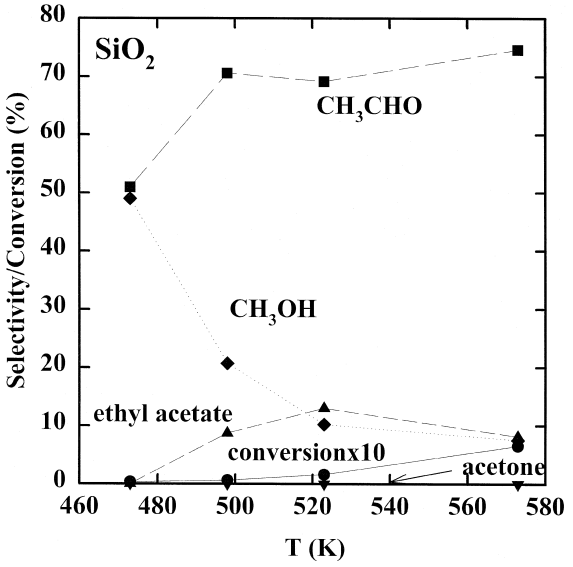


Fig. 5. Selectivity and conversion as a function of reaction temperature for ethanol reactions over $SiO_2$.

Fig. 1 presents Arrhenius plots of $k$ for the six catalysts examined in this work. The corresponding pre-exponential factor $A$ and apparent activation energy $E_a$ appear in Table 1. For comparison, Table 1 also lists literature values for $CeO_2$, CuO and $MoO_3$.

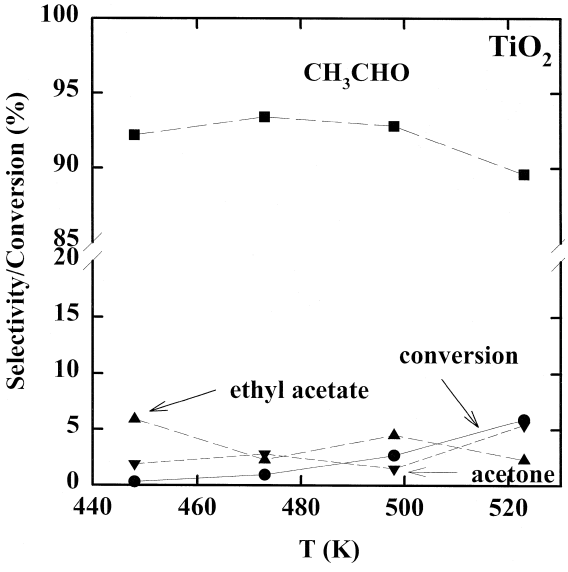


Fig. 4. Selectivity and conversion as a function of reaction temperature for ethanol reactions over $TiO_2$.

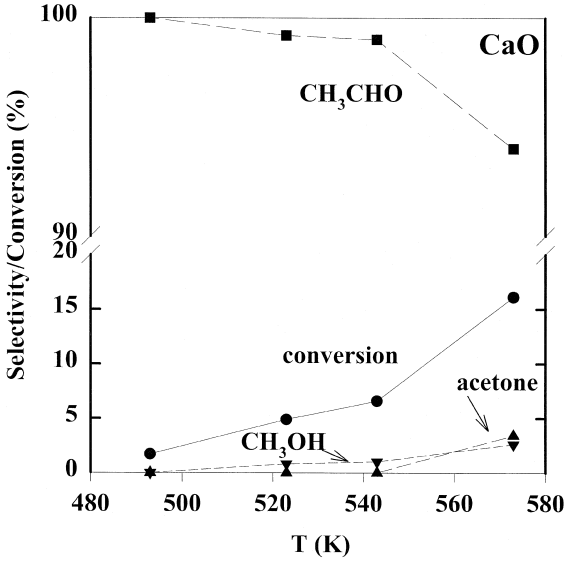


Fig. 6. Selectivity and conversion as a function of reaction temperature for ethanol reactions over CaO.

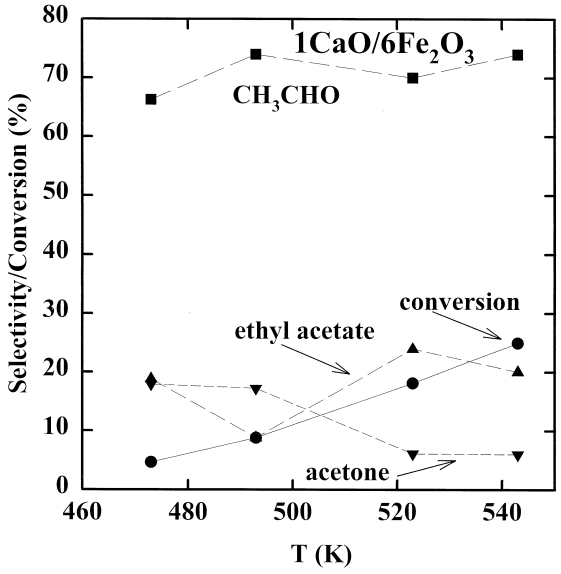


Fig. 7. Selectivity and conversion as a function of reaction temperature for ethanol reactions over 1 $CaO/6Fe_2O_3$.

In previous work [45] for reactions of the present type, we have found it useful to normalise *k* by the basic site density measured by $CO_2$ titration. Table 2 shows this density for the six oxides. Almost all the surfaces irreversibly adsorbed considerable amounts of $CO_2$. $SiO_2$ proved to be the lone exception; no $CO_2$ adsorbed even after pre-treating $SiO_2$ surfaces with air at 600 K for 1 h.

### *3.2. Selectivities*

Figs. 2–7 present carbon conversions, and selectivities for the various oxides examined here. All produced acetaldehyde as the principal product. $Fe_2O_3$ yielded appreciable amounts of ethyl acetate that decreased with increasing reaction temperature in favour of acetaldehyde (Fig. 2). $Fe_3O_4$ (Fig. 3) was more selective for acetaldehyde production at all conversions, but less active than $Fe_2O_3$. $SiO_2$ produced a great deal of methanol (particularly at low temperatures, Fig. 5) while $TiO_2$ (Fig. 4) and CaO (Fig. 6) yielded much less. Diethyl ether appeared in small quantities for $TiO_2$ and $SiO_2$ (not shown). Over $SiO_2$ significant amounts of crotonaldehyde appeared at high temperature (not shown in Fig. 5, but calculated to be 9.8% at 573 K). CaO yielded acetaldehyde as almost the sole product at all temperatures. The 1:6 $CaO/Fe_2O_3$ mixture resembled pure $Fe_2O_3$ except for producing much more acetone at low temperatures.

The selectivities in Figs. 2–7 correspond to fairly high conversions, and should be interpreted in only a qualitative sense since the sequential nature of the key reactions (as discussed below) make apparent selectivities vary with temperature. For better comparison of the major products, Table 3 lists measured selectivity to acetone, ethyl acetate and acetaldehyde extracted at conversions that all lie within the same range.

## 4. Discussion

### *4.1. Arrhenius parameters*

The pre-exponential factors in Table 1 lie in the $10^5$ ml/g s range except for $CeO_2$, where A is a factor of $10^4$ higher and for $SiO_2$, where it is $10^2$ lower. The apparent activation energies lie within about 15 kJ/mol of 63 kJ/mol except for $SiO_2$ and $MoO_3$, which fall appreciably higher. The deviation in parameters for $CeO_2$, $SiO_2$, and $MoO_3$ can be rationalized as follows.

Table 3
Low-conversion product selectivity (%) for ethanol oxidation

| Product (conversion, %) | CaO (1.7) $T = 493$ K | $TiO_2$ (0.94) $T = 473$ K | $Fe_3O_4$ (1.3) $T = 448$ K | $SiO_2$ (0.65) $T = 573$ K | $Fe_2O_3$ (1.62) $T = 433$ K |
|---|---|---|---|---|---|
| Acetaldehyde | 100 | 93.4 | 89.3 | 74.6 | 56.5 |
| Ethyl Acetate | 0 | 2.3 | 5.5 | 8.1 | 43.5 |
| Acetone | 0 | 2.8 | 5.2 | 0 | traces |

The abnormally high apparent activation energy for $MoO_3$ may be interpreted in light of reported structure-sensitivity effects for dehydration/dehydrogenation reactions on this oxide [18–22]. For example, loading low concentrations of $MoO_3$ on oxide supports like $SiO_2$ and $TiO_2$ decreases the apparent activation energy from 129 kJ/mol for pure $MoO_3$ to about 65 kJ/mol [18], which is within the normal range in Table 1. Particle size appears to play a key role through the heat of adsorption $\Delta H$. The apparent reaction activation energy $E_{app}$ comprises the true reaction activation energy $E$ for the rate-determining step together with $\Delta H$ according to:

$$E_{app} = E + (1 - m)\Delta H \quad (3)$$

where $m$ denotes the Bronsted transfer coefficient, which is less than unity. Since ethanol adsorption on most oxides is exothermic, $\Delta H$ is negative. Thus, increasing the magnitude of $\Delta H$ tends to make $E_{app}$ decrease. Such an effect appears to occur with decreased loading of $MoO_3$. Zhang et al. [18] have shown a decrease of 40 kJ/mol with decreasing the loading of $MoO_3$, which presumably decreases the particle size. This observation indicates that $\Delta$H changes with oxide particle size and dispersion. Interestingly, the observed rate of reaction for small and large particles remains roughly constant [18], suggesting that a decrease in the pre-exponential factor offsets the decrease in the apparent activation energy.

Ethanol reactions over $SiO_2$ have received relatively less attention in the literature. For $SiO_2$ prepared from ethyl orthosilicate (for purity), it has been reported that prior heating of the $SiO_2$ to 870 K or above can enhance the dehydrogenation pathway due to removal of surface silanol groups [41]. The silanol removal increases surface basicity, which in turn enhances the dehydrogenation reaction. The $SiO_2$ used in the present work has not been heated to such high temperatures and should therefore be less basic. The decreased basicity probably explains the negligible adsorption capacity for $CO_2$ (see Table 2 and below) and the correspondingly negligible dehydrogenation activity.

Acetaldehyde production from ethanol involves several steps, as will be detailed below. However, several lines of evidence suggest that the principal contribution to the prefactor comes from surface reaction as opposed to acetaldehyde desorption or O–H bond dissociation. Acetaldehyde-TPD over $CeO_2$ has been conducted previously [46]. Unreacted acetaldehyde desorbed at 380 K. This in not specific to $CeO_2$, other oxides have shown similar behaviour during acetaldehyde-TPD. The list includes $TiO_2$(001) single crystal [47], $TiO_2$ powder [47], $Cu/ZnO/Al_2O_3$ catalysts [48], β-$UO_3$ powder [49], and $Al_2O_3$ powder [49]. In other words, the oxidative dehydrogenation reactions at the elevated temperatures in this work and in Ref. [23] are not desorption limited. The very high preexponential factor translates into an extraordinarily large reaction rate because the apparent activation energy lies within the range of the other oxides. The relationship between the prefactor, activation energy, polarisability and the rate constants for this reaction, over a series of oxides, is treated in a separate work [44]. This present work is devoted to the understanding of the reaction pathway that, we believe, is an essential step before any more elaborate study [44].

### *4.2. Rate normalization by $CO_2$ uptake*

Fig. 8 shows Arrhenius plots for k normalised by the measured basic site densities. The data for the different solids collapse onto one line, strongly suggesting that basic sites contribute to the reaction and that one can use the $CO_2$ adsorption uptake to calculate turnover numbers.

Unfortunately, this normalisation fails for $SiO_2$, which does not adsorb any $CO_2$. More surprisingly, the normalisation also fails for CaO. Recently, $CO_2$ chemisorption on CaO surfaces has been studied by Metastable Impact Electron Spectroscopy, UPS and XPS [50]. The

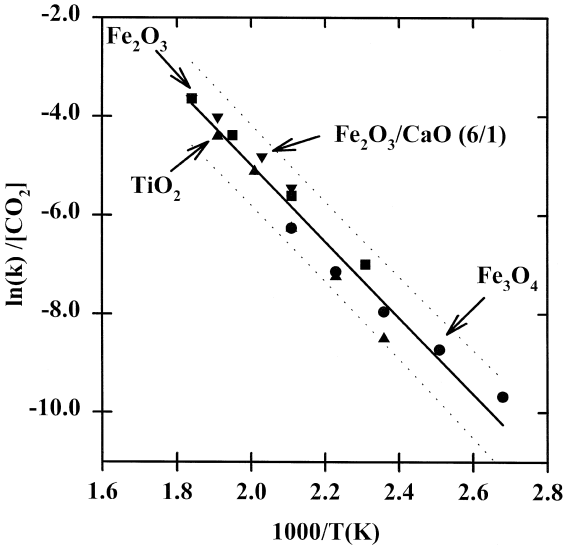


Fig. 8. Arrhenius plots of rate constant $k$ (ml/mol $CO_2$ s) for ethanol conversion normalised by amount of $CO_2$ adsorbed. This procedure in effect normalises by basic site density, and yields a single plot for the oxides shown.

authors found that $CO_2$ reacts very strongly with CaO; in fact their data indicate that $CO_2$ reacts with almost every available O site, not just the basic sites. (We attribute the relatively good normalization for the $Fe_2O_3$/CaO mixture to the low loading of CaO).

Curiously, CaO chemisorbs two orders of magnitude more $CO_2$ than does MgO [50–52], even though the two oxides have similar structure. Theoretical work based on cluster calculations has addressed this problem [53,54]. On MgO, $CO_2$ is predicted to chemisorb at four-fold coordinated $O^{2-}_{4c}$ step sites. The interaction of surface oxygen with $CO_2$ involves charge transfer from the uppermost filled O(2p) states into the vacant $\pi^*_u$ MO of $CO_2$. This transfer occurs most easily at a defect site with low coordination, like the $O^{2-}_{4c}$. CaO behaves very differently, however. Chemisorption occurs indiscriminately on regular $O^{2-}_{5c}$ sites of the CaO surface, mainly as a consequence of a very diffuse electronic cloud surrounding $O^{2-}$ anions as compared to those of MgO. These diffuse orbitals on CaO can overlap more efficiently with the $\pi^*_u$ orbital of $CO_2$. Thus, the adsorption data in Table 2 (and in Ref. [50]) agree perfectly with the cluster calculations [53,54].

## 5. Reaction mechanisms

Here we discuss the formation mechanisms for the three products observed most commonly in significant amounts: acetaldehyde, acetone, and ethyl acetate.

### 5.1. Acetaldehyde

Formation of acetaldehyde by the oxidative dehydrogenation of ethanol depends critically upon the reaction step that requires the oxide surface to acquire a negative charge. It is well accepted that upon adsorption, the O–H bond of the alcohol dissociates heterolytically to yield an ethoxide and a proton as follows:

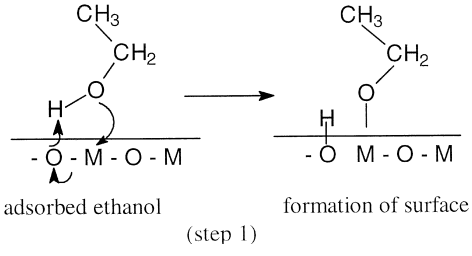


(4)

The amount of ethoxide does not necessarily correlate with catalytic activity. For example, considerable amounts of ethoxy species are observed at room temperature on oxides like $SiO_2$ [55], even though $SiO_2$ has very weak activity for oxidative dehydrogenation. Instead, the amount of ethoxide correlates with the number of metal cations that exhibit coordinative unsaturation. Any polycrystalline surface exhibits some of this unsaturation. Furthermore, the amount of ethoxide probably correlates with electronic charge distributions around the oxygen anions that tend to abstract the *H* as a proton.

TPD experiments have shown that electron donation to the surface via the oxygen lone

pairs of ethanol in step 1 is actually reversible [8,33–36] and proceeds as follows:

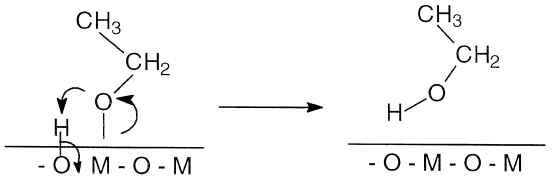


0Protonation of ethoxides (step 1') ethanol formation (5)

Ethoxides that do not disappear via step 1′ undergo dehydrogenation with subsequent electron donation to the cation, yielding acetaldehyde as follows:

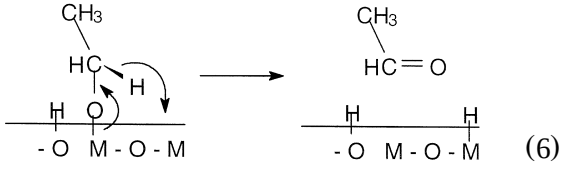


(6)

dehydrogenation (step 2) acetaldehyde formation

This picture shows why surfaces that promote oxidative dehydrogenation reactions tend to be those containing reducible (and reoxidisable) cations. Sometimes, however, step 2 proceeds quite slowly. In other words, it is the rate-determining step [18,56,57].

The residual hydrogen from ethanol adsorption generally desorbs either as $H_2O$ or as $H_2$. $H_2O$ can originate from the recombination of adsorbed OH and M–H. This product then desorbs, leaving an O vacancy and a partially reduced metal, which in presence of gas phase $O_2$ is reoxidised. Two adsorbed OH species can also combine to make one molecule of $H_2O$, one oxygen vacancy, and one restored oxygen anion site. On the other hand, two M–H species may combine to make $H_2$. We followed production of neither $H_2O$ nor $H_2$ in this work. However, considerable amounts of $H_2$ from alcohol oxidation has been reported elsewhere [58], although usually at higher temperatures than those employed here. Furthermore, we note that depending on the nature of the oxide, $H_2$ may be easily oxidised to $H_2O$ because of the rich $O_2$ environment.

### 5.2. Acetone

Acetone represents a further oxidation of the first reaction product acetaldehyde. This process probably begins with the formation of acetate species from acetaldehyde through oxidation by surface oxygen as follows:

$$CH_3CHO(a) + O(s) \rightarrow CH_3COO(a) + H(a) \quad (7)$$

Experiments on $TiO_2$ and Fe oxides [59,60] show that acetone can form naturally once surface acetate appears. The reaction probably proceeds via ketonization of two acetates as follows:

$$2CH_3COO(a) \rightarrow CH_3C(O)CH_3 + CO_2 + O(s) \quad (8)$$

Here, O(s) denotes oxygen incorporated into the surface.

There are two requirements for this reaction sequence to occur. First, the surface must be capable of donating its oxygen to adsorbed acetaldehyde in Eq. (6). This requirement suggests why $SiO_2$ shows no activity towards acetone formation. This oxide has little oxidising capability because of the great strength of the Si–O bond as well its relatively low electronic polarisability of 1.4 $Å^3$. Not surprisingly, infrared absorption data have never shown the presence of carboxylates developing from alcohols on clean $SiO_2$ surfaces.

The second requirement for acetone formation is that one surface cation must be able to accommodate two acetate molecules. Otherwise, the reaction of Eq. (7) cannot proceed. Such accommodation has been observed on $TiO_2$ (001) single crystals exhibiting a special faceting structure [59,61]. This structure exhibits {114}-facets that contain $Ti^{+4}$ cations. One third of

them are four-fold coordinated to oxygen as opposed to the usual six observed in the bulk.

$Fe_2O_3$ appears to behave similarly. Indeed, Fe oxide powders are known for their activity in making ketones from carboxylates [60]. The predominant natural growth face of the corundum-structured α phase of $Fe_2O_3$ is the (0001) basal plane [62]. The ideal surface structure remains nonpolar and contains Fe cations coordinated to only three oxygen anions. This structure represents only one-half of bulk cation coordination, and offers three-fold coordinative unsaturation. Not surprisingly, studies by low-energy electron diffraction have detected several reconstructions that increase the average coordination number [63–66]. Nevertheless, it is still very likely that $Fe^{+3}$ cations are present having the two-fold coordinative unsaturation required for Eq. (8). Unfortunately, we are aware of no surface science data regarding the reactions of alcohols or aldehydes on $Fe_2O_3$ single crystals to confirm this hypothesis. We can only point to the production of acetone from $Fe_2O_3$ in our own experiments.

$Fe_3O_4$ has an inverse spinel structure with $Fe^{2+}$ in octahedral sites and $Fe^{3+}$ distributed equally between octahedral and tetrahedral sites. The predominant natural growth faces are the (111) and (110) [62]. The (110) predominant face of $Fe_3O_4$ is expected to reconstruct due to the presence of large dipole fields [62]. Thus, surface instability leading to reconstruction is highly likely for $Fe_3O_4$ and may provide the required two vacant coordination sites for the coupling reaction. Again, however, we are aware of no pertinent experiments regarding the reactions of oxygenates on $Fe_3O_4$, but our own experiments do show acetone formation (though at a rate 2.5 times lower than for $Fe_2O_3$).

We note that the distinction between the surface of $Fe_2O_3$ and that of $Fe_3O_4$ may not be straightforward. For example, LEED and STM reports indicate that $Fe_3O_4$(111) layers are formed at the surface of α-$Fe_2O_3$ (0001) single crystals depending on the annealing temperatures [67,68].

In contrast to all these cases, the absence of acetone formation on CaO probably (at low temperatures) results from a lack of coordinative unsaturation. (The abundance of acetaldehyde formed by CaO shows that the reaction of Eq. (6) proceeds without difficulty). CaO has the rocksalt structure, with cations six-fold coordinated to oxygen in the bulk. CaO exhibits perfect cleavage along the (100) direction, and quantitative LEED *I–V* measurements have shown that the surface represents a nearly exact termination of the bulk structure [69]. Thus, $Ca^{2+}$ can coordinate only singly. Cluster calculations have shown that carbonates formed from $CO_2$ and $O^{2-}$ are monodentate, so by analogy one may expect that carboxylates from acetaldehyde will also be bond in a monodendate configuration on the surface. We are aware of no data for aldehyde reactions on well-defined single crystals of CaO, so this idea cannot be confirmed directly. However, pertinent data do exist for MgO (100) [70,71], another oxide having the rocksalt structure and having a bond strength close to that of CaO. These results indicate that aldehydes undergo Cannizzaro-type disproportionation reaction to carboxylates and alkoxides instead of coupling to ketones.

As we pointed out in the Results, quantitative rate analysis of the reactions in Eqs. (7) and (8) is difficult given the overall rate data we collected in our experiments. Since acetone forms from acetaldehyde, the reaction yield by itself offers limited insight into the activity of the oxide toward ketonization. However, a ketonization rate constant can be calculated under the assumption that the key step obeys:

$$2CH_3CHO(a) + 2O(s) \rightarrow CH_3C(O)CH_3 + CO_2 + H_2O \quad (9)$$

Then the rate can be expressed as:

$$r = k[CH_3CHO]^2[\text{Oxide}] = k'[CH_3CHO]^2 \quad (10)$$

where $k' = k$ [Oxide]. Table 4 presents results for $k'$ computed this way at 473 K. $TiO_2$ is the

Table 4
Rate constants at 473 K

| Oxide | $k_{Acetone}$ ($ml^2/(g\ s\ mol)$) | $k_{Ethyl\ Acetate}$ ($ml^2/(g\ s\ mol)$) |
|---|---|---|
| $TiO_2$ | $7.3\times10^5$ | $5.9\times10^5$ |
| $Fe_2O_3$ | $5.1\times10^5$ | $18.7\times10^5$ |
| $Fe_3O_4$ | $2.0\times10^5$ | $4.6\times10^5$ |

most active catalyst, followed by $Fe_2O_3$ and $Fe_3O_4$. Neither $SiO_2$ nor CaO show any activity.

### 5.3. Ethyl acetate

Ethyl acetate represents the second most important reaction product in our experiments. We suspect that ethyl acetate forms via the Tishchenko reaction.

This sort of ester formation from aldehydes has been reported on the surfaces of several oxides, including U oxides [72], $SnO_2$-based catalysts [72], and Cu/Zn/Al catalysts [48]. Eq. (11) suggests that the reaction is second order in acetaldehyde. Thus, a rate constant for this reaction can be computed in the same manner as for acetone. Table 4 shows the rate constant for ethyl acetate production at 473 K obtained this way for the pure oxides. The progression mimics that for acetone, except that now $Fe_2O_3$ is more active than $TiO_2$. The Tishchenko reaction requires *H* transfer from one adsorbed acetaldehyde, which becomes oxidised, to another adsorbed acetaldehyde, which is reduced to alkoxide. This process may form a complex in a transition state that requires participation of the surface oxygen:

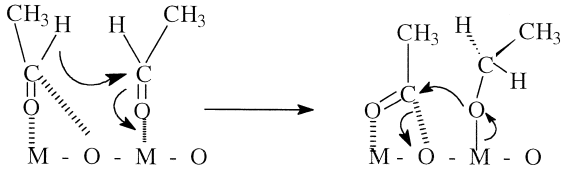


$$\rightarrow \quad CH_3CH_2OC(O)CH_3 \qquad (11)$$

where an adsorbed acetaldehyde molecule with the participation of a surface oxygen anion transfers a hydride to another adsorbed acetaldehyde molecule. This results in a weakly formed acetate species in proximity of an ethoxide species; most likely in an unstable configuration. Both species react together yielding an ethylacetate molecule and liberating the surface oxygen.

Table 2 shows that $Fe_2O_3$ adsorbs three times more $CO_2$ than does $TiO_2$; in other words $Fe_2O_3$ is more basic than $TiO_2$. It is thus not surprising that $Fe_2O_3$ is more active than $TiO_2$ for this reaction. Quantitatively speaking, however, we attribute no special significance to the correspondence between the three-fold increase in *k* (Table 4) and the three-fold increase in $CO_2$ adsorption (Table 2) for $Fe_2O_3$ when compared to $TiO_2$. We regard the agreement as fortuitously good.

## 6. Conclusions

Oxidative dehydrogenation of ethanol over a variety of oxides yields acetaldehyde as the primary product, and (usually) acetone and ethyl acetate as products of further oxidation of acetaldehyde. This observation falls largely in line with previous work for a smaller number of other oxides. The Arrhenius parameters we have measured also fall mostly in the same range. We have rationalized the mechanism for acetaldehyde formation in terms of the capacity of surface metal cations to be easily reduced and reoxidised. However, our data together with ultrahigh vacuum work from other laboratories suggest that continued oxidation of acetaldehyde to acetone depends upon the presence of coordinative unsaturation of the metal cations. Basic site density, as monitored by $CO_2$ adsorption, can be used successfully to normalize the reaction rate of these oxides with the exception of CaO. This exception can be explained by reference to cluster calculations [53,54].

## Acknowledgements

E.G.S. gratefully acknowledges a Sloan Foundation Fellowship. This work was partially supported by the National Science Foundation under a Presidential Young Investigator Award.

## References

[1] J. Franckaerts, G.F. Froment, Chem. Eng. Sci. 19 (1964) 807.
[2] A. Pelso, M. Moresi, C. Mustachi, B. Soraccco, Can. J. Chem. Eng. 57 (1979) 159.
[3] J. Edwards, J. Nicollaidis, M.B. Cultip, C.O. Bennett, J. Catal. 50 (1977) 24.
[4] McGraw-Hill Encyclopedia of Science and Technology, 8th edn., Vol. 6, McGraw-Hill, NY 1997, p. 566.
[5] T.L.F. Favre, G. van der Lee, V. Ponec. J. Chem. Cos. Chem. Commun. (1985) 230.
[6] M. Ichikawa, Bull. Chem. Soc. Jpn. 51 (1978) 2273.
[7] A. Kiennemann, J.P. Hindermann, R. Breault, H. Idriss, Am. Chem. Soc., Reprints Symp. on Chemicals from Syngas and Methanol 31 (1) (1986) 46.
[8] C. Diagne, H. Idriss, J.P. Hindermann, A. Kiennemann, Appl. Catal. 51 (1989) 165.
[9] J.E. Baker, R. Burch, S.E. Golunski, Appl. Catal. 53 (1989) 279.
[10] H. Rajesh, U.S. Ozkan, Ind. Eng. Chem. Res. 32 (1993) 1622.
[11] J.J. Foster, R.I. Masel, Ind. Eng. Chem. Res. 25 (1986) 2556.
[12] W.L. Faith, D.B. Keyes, R.L. Clark, Industrial Chemicals, 2nd edn., Wiley, New York, 1957, pp. 2–3.
[13] Y.-J. Tu, C. Li, Y.-W. Chen, J. Chem. Tech. Biotechnol. 59 (1994) 141.
[14] N. Doca, E. Segal, React. Kinet. Catal. Lett. 28 (1985) 123.
[15] N. Doca, E. Segal, Rev. Roumaine. Chim. 31 (1986) 567.
[16] N. Kanoun, M.P. Asteir, G.M. Pajonk, Appl. Catal. 70 (1991) 225.
[17] H. Zhou, J.Y. Wang, X. Chen, C.-L. O'Young, S.L. Suib, Microporous Mesoprous Mater. 21 (1998) 315.
[18] W. Zhang, A. Desikan, T. Oyama, J. Phys. Chem. 99 (1995) 14468.
[19] J.-M. Tatibouët, J.-E. Germain, J. Chem. Res. S (1981) 268.
[20] T. Ono, H. Kamisuki, H. Hisashi, H. Miyata, J. Catal. 116 (1989) 303.
[21] Y. Iwasawa, Y. Nakano, S. Ogaswara, J. Chem. Soc. Faraday Trans. 1 74 (1978) 2986.
[22] W.E. Farneth, R.H. Staley, A.W. Sleight, J. Am. Chem. Soc. 108 (1986) 2327.
[23] S. Morrison, in: A. Yee, S. Morrison, H. Idriss, MSc Thesis, The University of Auckland, 1998, J. Catal. (1999) in press.
[24] H. Tsuji, F. Yagi, H. Hattori, H. Kita, J. Catal. 148 (1994) 759.
[25] K. Weissermel, H.-J. Arpe, Industrial Organic Chemistry, Verlag Chemie, 1978, p. 94.
[26] Design News, June 22, 1998.
[27] H. Noller, J.A. Lercher, H. Vinek, Mater. Chem. Phys. 18 (1988) 577.
[28] A.M. Youssef, L.B. Khalil, B.S. Girgis, Appl. Catal. A 81 (1992) 1.
[29] S.M. Gates, J.N. Russell, J.T. Yates Jr., Surf. Sci. 171 (1986) 111.
[30] G.L. Nyberg, S.E. Anderson, Surf. Sci. 207 (1989) 253.
[31] J. Xu, X. Zhang, R. Zenobi, J. Yoshinobu, Z. Xu, J.T. Yates Jr., Surf. Sci. 256 (1991) 288.
[32] J.L. Davis, M.A. Barteau, Surf. Sci. 187 (1987) 387.
[33] Y. Cong, V. van Spaendonk, R.I. Masel, Surf. Sci. 385 (1997) 246.
[34] K.S. Kim, M.A. Barteau, W.E. Farneth, Langmuir 4 (1988) 533.
[35] V.S. Lusvardi, M.A. Barteau, W.E. Farneth, J. Catal. 153 (1995) 41.
[36] V.S. Lusvardi, M.A. Barteau, W.R. Dollinger, W.E. Farneth, J. Phys. Chem. 100 (1996) 18183.
[37] J.B. Benziger, in: E. Shustarovich (Ed.), Metal-Surface Reaction Energetics, VCH, New York, 1991.
[38] D.G. Rethwisch, J.A. Dumesic, Appl. Catal. 21 (1986) 97.
[39] K.S. Kim, M.A. Barteau, Surf. Sci. 223 (1989) 13.
[40] M.A. Barteau, Chem. Rev. 96 (1996) 1413.
[41] Y. Matsumura, K. Hashimoto, S. Yoshida, J. Chem. Soc., Chem. Commun. (1987) 1599.
[42] I. Halasz, H. Vinek, K. Thomke, H. Noller, Z. Phys. Chem. 163 (1985) 157.
[43] A. McKenze, C. Fishel, R. Davis, J. Catal. 138 (1992) 547.
[44] H. Idriss, E.G. Seebauer, in preparation.
[45] H. Idriss, E.G. Seebauer, J. Vac. Sci. Technol. A 14 (1996) 1627.
[46] H. Idriss, C. Diagne, J.P. Hindermann, A. Kiennemann, M.A. Barteau, J. Catal. 155 (1995) 219.
[47] H. Idriss, K.S. Kim, M.A. Barteau, J. Catal. 139 (1993) 119.
[48] A. Kiennemann, H. Idriss, R. Kieffer, P. Chaumette, D. Durand, Ind. Eng. Chem. Res. 30 (1991) 1130.
[49] H. Madhavaram, H. Idriss. in preparation.
[50] D. Ochs, B. Braun, W. Maus-Friedrichs, V. Kempter, Surf. Sci. 417 (1998) 406.
[51] D. Ochs, B. Braun, W. Maus-Friedrichs, V. Kempter, Surf. Sci. 397 (1998) 184.
[52] D. Ochs, B. Braun, W. Maus-Friedrichs, V. Kempter, J. Electron. Spectrosc. Relat. Phenom. 88 (1998) 757.
[53] G. Pacchionni, Surf. Sci. 281 (1993) 207.
[54] G. Pacchionni, J.M. Ricart, F. Illas, J. Am. Chem. Soc. 116 (1994) 10152.
[55] J. Raskò, J. Bontovics, F. Solymosi, J. Catal. 146 (1994) 22.
[56] R.S. Weber, J. Phys. Chem. 98 (1994) 2999.
[57] N. Koga, S. Obara, K. Kitaura, K. Morokuma, J. Am. chem. Soc. 107 (1985) 7109.
[58] M.L. Cuberio, J.L. Fierro, J. Catal. 179 (1998) 150.
[59] K.S. Kim, M.A. Barteau, J. Catal. 125 (1990) 353.
[60] E.J. Grootendorst, R. Pestman, R.M. Koster, V. Ponec, J. Catal. 148 (1994) 261.
[61] H. Idriss, K.S. Kim, M.A. Barteau, Stud. Surf. Sci. Catal. 64 (1991) 327.
[62] V.E. Henrich, P.A. Cox, The Surface Chemistry of Metal Oxides, Cambridge Univ. Press, 1994; and references therein.
[63] C. Sanchez, K.D. Hendewerk, K.D. Sieber, G.A. Somorjai, J. Solid State Chem. 61 (1986) 47.

[64] M.F. Hochella Jr., C.M. Eggleston, V.B. Elings, G.A. Parks, G.E. Brown Jr., C.M. Wu G.E, K. Kjoller, Am. Mineral. 74 (1989) 1233.
[65] P.A. Johnsson, C.M. Eggleston, M.F. Hochella Jr., Am. Mineral. 76 (1991) 1442.
[66] C.M. Eggleston, M.F. Hochella Jr., Am. Mineral. 77 (1992) 911.
[67] R.J. Lad, V.E. Henrich, Surf. Sci. 193 (1988) 81.
[68] N.C. Condon, P.W. Murray, F.M. Leibsle, G. Thornton, A.R. Lennie, D.J. Vaughan, Surf. Sci. 310 (1994) L609.
[69] M. Prutton, J.A. Walker, M.R. Welton-Cook, R.C. Felton, J.A. Ramsey, Surf. Sci. 89 (1979) 95.
[70] X.D. Peng, M.A. Barteau, Langmuir 5 (1989) 1051.
[71] X.D. Peng, M.A. Barteau, Surf. Sci. 224 (1989) 327.
[72] M. Ai, J. Catal. 83 (1983) 141.
[73] J.E. Rekoske, M.A. Barteau, J. Catal. 165 (1997) 57.